

RESEARCH LETTER

10.1029/2018GL078429

Key Points:

- Multiyear surface velocity data of the Florida Current and East Australian Current are compared at 1 km/1 hr scales with high frequency radar
- Despite contrasting local wind, bathymetry, and meandering, the time-mean structure of their jet speed and lateral shear are almost identical
- Eddy kinetic energy submesoscale wavenumber spectra are steep, with weak seasonal variability across both upstream western boundary currents

Supporting Information:

- Supporting Information S1

Correspondence to:

M. R. Archer,
matthew.robert.archer@gmail.com

Citation:

Archer, M. R., Keating, S. R., Roughan, M., Johns, W. E., Lumpkin, R., Beron-Vera, F. J., & Shay, L. K. (2018). The kinematic similarity of two western boundary currents revealed by sustained high-resolution observations. *Geophysical Research Letters*, 45, 6176–6185. <https://doi.org/10.1029/2018GL078429>

Received 18 APR 2018

Accepted 31 MAY 2018

Accepted article online 8 JUN 2018

Published online 25 JUN 2018

The Kinematic Similarity of Two Western Boundary Currents Revealed by Sustained High-Resolution Observations

M. R. Archer¹ , S. R. Keating¹ , M. Roughan^{1,2,3} , W. E. Johns⁴, R. Lumpkin⁵ ,
F. J. Beron-Vera⁶ , and L. K. Shay⁴

¹University of New South Wales (UNSW), School of Mathematics and Statistics, Sydney, New South Wales, Australia, ²UNSW, School of Biological Earth and Environmental Sciences, Sydney, New South Wales, Australia, ³MetOcean Solutions (Meteorological Service of New Zealand), New Plymouth, New Zealand, ⁴University of Miami, Department of Ocean Sciences, Rosenstiel School of Marine and Atmospheric Science (RSMAS), Miami, FL, USA, ⁵NOAA, Atlantic Oceanographic and Meteorological Laboratory, Miami, FL, USA, ⁶University of Miami, Department of Atmospheric Sciences, RSMAS, Miami, FL, USA

Abstract Western boundary currents (WBCs) modulate the global climate and dominate regional ocean dynamics. Despite their importance, few direct comparisons of the kinematic structure of WBCs exist, due to a lack of equivalent sustained observational data sets. Here we compare multiyear, high-resolution observations (1 km, hourly) of surface currents in two WBCs (Florida Current and East Australian Current) upstream of their separation point. Current variability is dominated by meandering, and the WBCs exhibit contrasting time-mean velocities in a Eulerian coordinate frame. By transforming to a jet-following coordinate frame, we show that the time-mean surface velocity structure of the WBC jets is remarkably similar, considering their distinct local wind, bathymetry, and meandering signals. Both WBCs show steep submesoscale kinetic energy wavenumber spectra with weak seasonal variability, in contrast to recent findings in other ocean regions. Our results suggest that it is the mesoscale flow field that controls mixing and ocean dynamics in these regions.

Plain Language Summary Western boundary currents (WBCs) are warm, strong currents that flow along the western sides of the world's ocean basins. They dominate the climate and ecology of some of the most densely populated coastlines on Earth. Considering their importance, there is surprisingly little knowledge of how different WBCs compare. In this paper we use high-resolution measurements to study the mean structure and variability of two WBCs, in the North Atlantic and South Pacific, and show that while they differ in their variability, they are remarkably similar in their time-mean. We discovered this by transforming the coordinate frame in which we viewed them, so that the variability of the meandering currents does not affect the mean calculation. We quantify the amount of variability at different spatial scales and show that for these WBC regions, variability is dominated by the large-scale flow field, with no seasonal cycle at the smaller scales, in contrast to studies of other ocean current regimes. These high-resolution results provide an updated view of WBC systems globally and can be used by numerical modelers to evaluate the performance of their models, helping to improve forecasts of a changing climate.

1. Introduction

Western boundary currents (WBCs) are warm, narrow, and intense currents that flow poleward along the western edge of ocean basins, balancing the equatorward wind-driven transport in the open ocean. WBCs and their eddy field modulate Earth's climate by exporting heat from the tropics toward the poles and mediate large air-sea heat and moisture fluxes that fuel midlatitude storms (Yu & Weller, 2007). They also act as a sink for carbon dioxide via subduction and biological uptake (Cronin et al., 2010; Ducklow et al., 2001). At the regional level, WBCs play a critical role in shelf circulation and coastal ecology, mixing water masses and upwelling nutrients into the sunlit surface layers where they are utilized by ecological communities (Lee et al., 1981; Shulzitski et al., 2015) and commercial fisheries (Richardson et al., 2009).

Because of their importance, significant effort has been invested to monitor the structure and variability of WBCs (see review by Imawaki et al., 2013). Such observational data sets provide insight into the influence of WBCs in both global and regional circulation, helping to constrain numerical ocean models. However, there are still many open questions, especially at scales of $O(1-10)$ km that are highly relevant to the biogeochemistry and productivity of continental shelf regions (Mahadevan, 2016). These scales, termed

submesoscale, differ dynamically from larger mesoscale flows as they are (i) below the first baroclinic Rossby radius of deformation, (ii) exhibit vertical velocities as large as 100 m/d, and (iii) are associated with $O(1)$ Rossby number ($Ro = V/fl$, where V is an rms velocity, f the local Coriolis frequency, and l the horizontal length scale), indicating the importance of advection in the force balance (McWilliams, 2016). Recent observations reveal seasonality in the submesoscale flow field over the open ocean and WBC extensions (Callies et al., 2015; Qiu et al., 2017), with a more energetic submesoscale eddy kinetic energy (EKE) field during wintertime. As yet there have been no observational studies of submesoscale seasonality in WBCs upstream of their separation point, where the dynamics are strongly anisotropic and dominated by the presence of the jet (Schaeffer et al., 2017).

Here we make the first detailed comparison of two upstream WBCs—the Florida Current (FC) in the northern hemisphere and the East Australian Current (EAC) in the southern hemisphere—using multiyear observations of surface currents at hourly/kilometer scales from high frequency (HF) radar (Paduan & Washburn, 2013). These complementary data sets offer unprecedented views of the two WBC jets as they flow along the eastern coastlines of the U.S. and Australia, respectively. Whereas a mooring array typically resolves $O(10)$ grid points in a cross-jet direction, HF radar resolves $O(1)$ -km scale grid points over a range of 100 km in both cross-jet and along-jet directions. This high spatial resolution allows us to accurately track the jets as they meander across the continental slope and resolve frontal eddies and other instabilities in 2-D (e.g., Archer, Shay, Jaimes, et al., 2015; Mantovanelli et al., 2017; Shay et al., 1998; Schaeffer et al., 2017). The two study regions are as follows:

1. The FC is the upstream branch of the Gulf Stream system that is constrained within the Florida Straits (Figure 1a). It flows northward following the narrow continental shelf (~3 km offshore Miami) and exits the Straits at 26°N, continuing along the shelf until it separates from the coastline at Cape Hatteras (32°N). Around 25°N the FC's mean core speed is ~1.6 m s⁻¹ located 40 km offshore (Archer, Shay, et al., 2017; Richardson et al., 1969). The FC has a volume transport of ~30 Sv with a standard deviation (STD) of 3 Sv (1 Sverdrup = 10⁶ m³ s⁻¹; Meinen et al., 2010). It undergoes a weak seasonal cycle in speed and volume transport (~10% of observed variance), with a maximum most commonly observed during boreal summer (Meinen et al., 2010). The FC exhibits largest variability at 2–30 days, due to local and regional wind stress, and lateral meandering with an amplitude of ~60 km and STD of 8 km (Archer, Shay, et al., 2017; Johns & Schott, 1987; Schott et al., 1988). Remote wind forcing, communicated via first mode baroclinic Rossby waves, has been shown to affect the annual cycle in volume transport (Domingues et al., 2016), but for the data presented here at 25–26°N, the Bahamas island chain blocks most of this direct mid-ocean influence (Archer, Shay, et al., 2017).
2. The EAC closes the South Pacific subtropical gyre, flowing poleward along SE Australia (Figure 1b). At 30°S the EAC flows over the continental slope about 30 km offshore. In contrast to the Gulf Stream, the EAC does not have one dominant separation region controlled by coastline geometry. Instead, the separation point ranges from 28 to 37°S, but 30–32°S about 50% of the time (Cetina-Heredia et al., 2014). At 30–31°S, the EAC has a mean core speed between 0.6 and 1.35 m s⁻¹ (Archer, Roughan, et al., 2017; Mata et al., 2000; Schaeffer et al., 2017) and a volume transport of ~22 Sv with an STD of ~5–7 Sv (Mata et al., 2000; Sloyan et al., 2016). The jet speed and EKE undergo a seasonal cycle with an austral summer maximum (Archer, Roughan, et al., 2017; Ridgway & Godfrey, 1997). The EAC meanders with a longer period than the FC, at 20–45 days, with a second dominant mode at 65–110 days associated with mesoscale eddy variability of the separation point (Bowen et al., 2005; Mata et al., 2000). The amplitude of EAC meandering is larger than the FC, with a lateral displacement from the mean over 80 km and STD of 20 km (Archer, Roughan, et al., 2017). Local wind forcing can drive sporadic upwelling and cross shelf transport in the EAC, but generally, current variability occurs on longer time scales and is a largely unrelated to local winds (e.g., Schaeffer et al., 2014, their Figure 10). Regional wind forcing can influence the timing of the EAC eddy shedding events, while remote wind forcing has limited impact on the intrinsically variable EAC system (Bull et al., 2017).

2. Data and Methods

Both WBCs were monitored with WERA phased-array HF radar systems (Gurgel et al., 1999; Shay et al., 2007). In the FC (Figures 1a and 1c), 2 years of data (January 2005 to December 2006) are analyzed from two sites

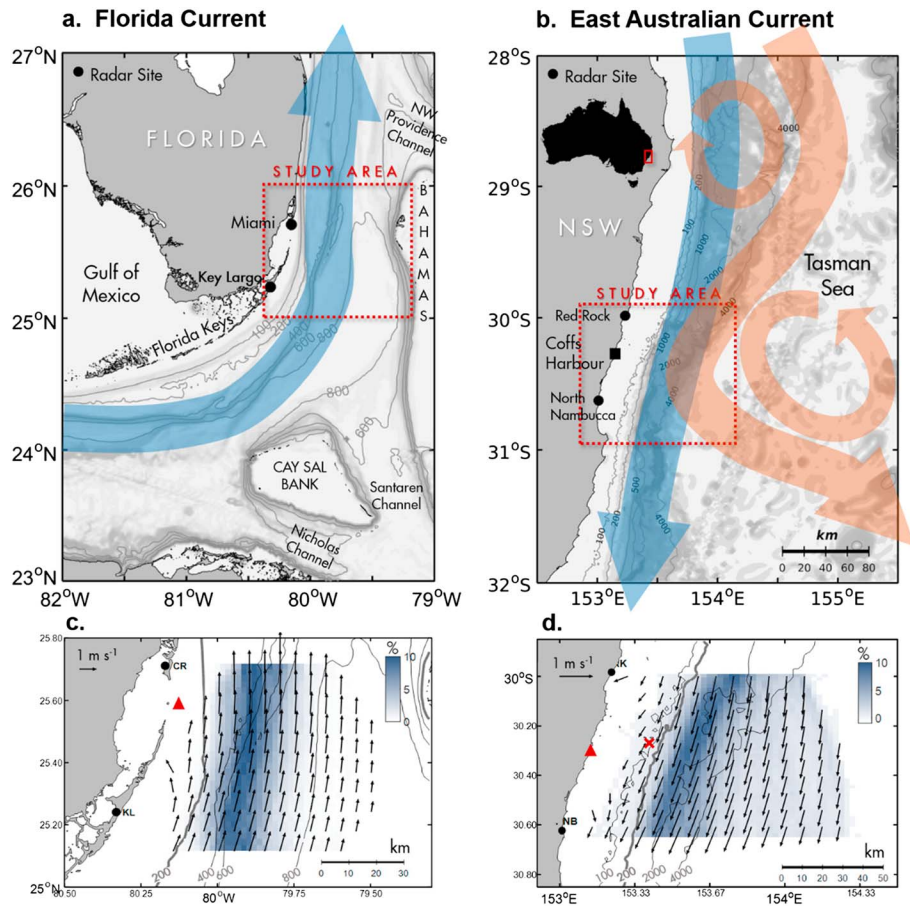


Figure 1. Maps of the western boundary current (WBC) systems. (a) The Florida Straits (USA), with the Florida Current (FC) in blue. (b) the Tasman Sea offshore New South Wales (NSW), Australia, with the East Australian Current (EAC) in meander mode separating from the shelf (orange) and nonmeander (blue). Study areas are depicted with a red-dashed box. (c and d) Mean velocity (black arrows), superimposed on a 2-D histogram of jet core location (frequency normalized each latitude to a %), for the FC and EAC, respectively. The red triangles show the wind measurement sites. The red cross in (d) shows the location of mooring CH100. The depth of isobaths is in meters, the thicker gray lines in (c) and (d) represent the 200-m isobath.

(Miami and Key Largo), operating at 16.045 MHz (Martinez-Pedraja et al., 2013; Shay et al., 2008). Vector velocities on a Cartesian 1.2-km resolution grid are calculated from quality controlled radials every 20 min with the unweighted least squares method of Gurgel (1994). To quality control the radial data, each grid point time series is smoothed with a 9-point (3 hr) Hann window. Data points exceeding 3 STD from a running 5 day mean and grid points with a STD over 0.5 m s^{-1} , or with less than 15% data coverage, are not included in the analysis (Archer, Shay, & Martinez-Pedraja, 2015). This data set is discussed in detail by Archer, Shay, et al. (2017).

In the EAC (Figures 1b and 1d), 4 years of HF radar data (March 2012 to July 2016) are analyzed from two sites operating at 13.92 MHz near Coffs Harbour (30–31°S), deployed as part of Australia's Integrated Marine Observing System (IMOS; Roughan et al., 2015; Wyatt et al., 2017). Each radial velocity data set is combined using the unweighted least squares method of Gurgel (1994) to a Cartesian grid with 1.5-km resolution at 10-min intervals smoothed with a 17-point (3 hr) Hann window. The time series is despiked by removing occurrences of consecutive data points separated by 0.8 m s^{-1} , and outliers over 3 STD from a 7-day mean and 3.5 STD from the total mean were removed. Full details are presented in Archer, Roughan, et al. (2017).

Subsurface current data from the EAC are obtained from a bottom-mounted ADCP deployed at the 100-m isobath (named CH100), within the HF radar footprint at 30.27°S (Figure 1d; Schaeffer et al., 2013). Current

velocity is measured at 4-m bin resolution between 13 and 89 m, every 5 min, and subsampled to 3 hr to match the HF radar data. Concomitant subsurface velocity data are not available for the FC.

Wind in the Florida Straits is measured at Fowey Rocks meteorological station, 8 km offshore Miami's Biscayne Bay (Figure 1c). In southeast Australia, wind measurements are taken from Coffs Harbour meteorological station (Figure 1d). Both data sets are subsampled to 3 hr to match HF radar measurements.

To control for meandering, HF radar data for each region were converted to a time-evolving jet coordinate frame (Archer, Shay, et al., 2017; Archer, Roughan, et al., 2017). In jet coordinates the position of the jet core is the origin of reference rather than a geographical location (Halkin & Rossby, 1985). In this frame, a time-mean representation of the jet is not contaminated by smearing of the meandering high velocity core, so higher core speeds and lateral shears are retained (see supporting information for more detail).

Eddy kinetic energy wavenumber power spectra are calculated over a subset of longitudinal (geographical frame) or cross-jet (jet frame) transects, for coverage >75%. Depending on time-variable data coverage, these transects are generally 30–70 km long, with a resolution of 1.2 km for the FC (1.5 km for the EAC). For each transect, data are linearly detrended, the time and space mean profile is subtracted, a Hann window is applied, and the Fourier transform calculated. The time mean is taken over the full observation record; we tested the sensitivity of different time windows (7 days, 30 days, and seasonal) and found that the variation does not significantly impact the mean wavenumber slopes. We average spectra over summer and winter. Summer (winter) is defined for the FC (EAC) as June–July–August, and winter (summer) is December–January–February. Frequency spectra are calculated only in geographical coordinates, since gaps are larger and more frequent in the jet coordinate time series (usually caused by insufficient data during the coordinate conversion). Spectral confidence levels were calculated using a χ^2 distribution (see supporting information).

3. Observations

3.1. Mean Jet Profiles

In geographical coordinates, the two WBCs have contrasting cross-jet profiles of mean speed (Figure 2a). The FC mean core speed is 1.5 m s^{-1} with STD of 0.35 m s^{-1} . In contrast, the EAC profile is weaker and more diffuse, with a mean core speed of 0.8 m s^{-1} and STD of 1.1 m s^{-1} . The velocity shear in the FC is twice that in the EAC, although both WBCs exhibit similar asymmetry in magnitude of cyclonic to anticyclonic shear (Figure 2b), as previously observed in the Gulf Stream (e.g., Rossby & Zhang, 2001).

In jet coordinates, the mean cross-jet velocity profile of the FC and EAC converge, with core speeds of 1.6 and 1.35 m s^{-1} , and STDs reduced to 0.2 and 0.3 m s^{-1} , respectively (Figure 2c). Even more striking is the similarity in the two jet's time-mean lateral shear profiles, which are almost identical (Figure 2d). The remaining difference in speed may be due to the FC carrying a component of the thermohaline circulation, with larger observed volume transport than the EAC, together with the spatial constraint of the relatively narrow and shallow Florida Straits. Differences in shear outside the core are also primarily because the FC is restricted by land on both sides, so anticyclonic shear must remain relatively large for v to reduce to zero at the Bahamas (Figure 1a). In contrast, the EAC has no bathymetric constraint east of the jet, so anticyclonic shear weakens with increasing distance from the core.

3.2. Temporal Variability of Currents

Surface current velocity fields of the EAC and FC exhibit similar power density spectral slopes of kinetic energy (KE), with a distinct peak at the principal lunar semidiurnal M_2 and a broader peak at the diurnal K_1 and O_1 frequencies (Figures 3c and 3d). In the EAC at 30.5°S the inertial period is 23.6 hr; in the FC at 25.5°N it is 27.9 hr, hence the broadband diurnal peak that contains near-inertial wave signals (Archer, Shay, Jaimes, et al., 2015; Shay et al., 1998). In these high geostrophic shear regions, near-inertial period motions can be shifted by the background vorticity so that they are closer to the diurnal period (e.g., Kunze & Toole, 1997). The critical latitude (at 30°N and S for no background vorticity) is where the local inertial period is close to diurnal forcing driven by tides and the land-sea breeze (e.g., Kim & Crawford, 2014; Mihanović et al., 2016; Simpson et al., 2002). Because of this, both data sets exhibit strong diurnal variability. However, in the mesoscale frequency range, the EAC exhibits much higher variability, associated with a more

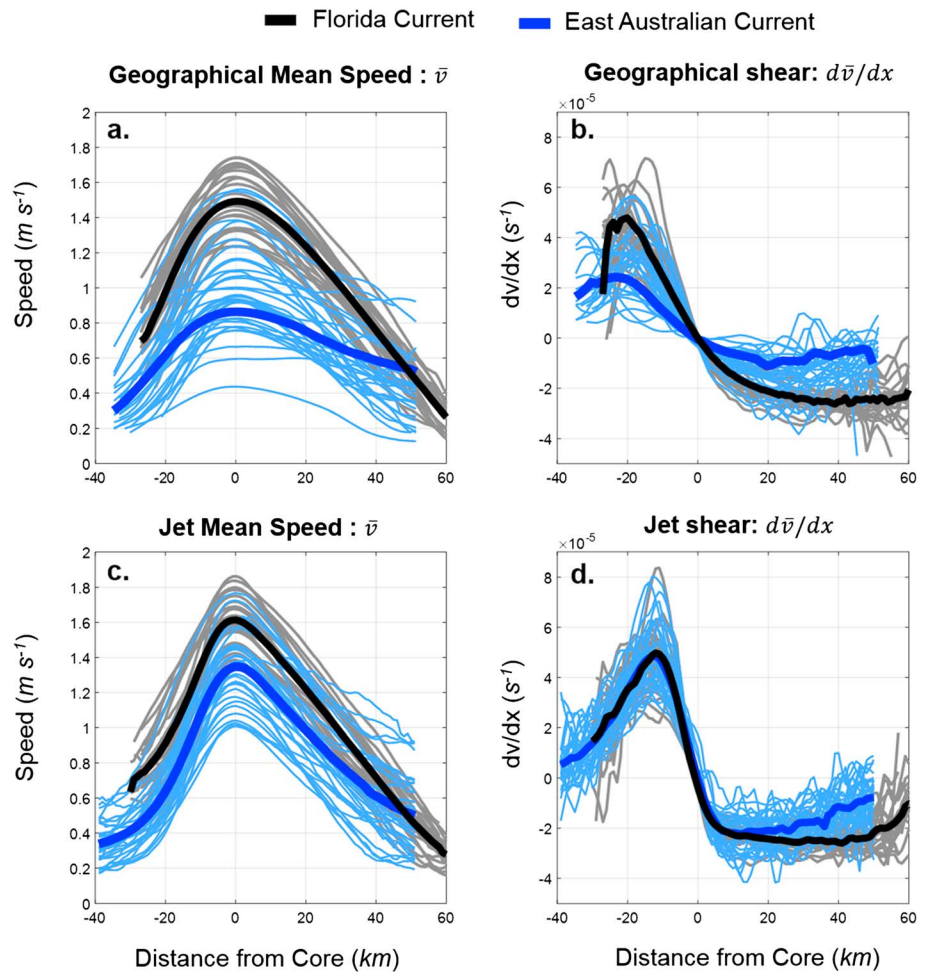


Figure 2. Time-mean cross-jet profiles of speed and lateral shear. (a) Geographical coordinate frame speed; (b) geographical shear; (c) jet coordinate frame speed; (d) jet shear. The thin lines represent all monthly averages for the observation periods; the thick lines represent the total time mean.

energetic meandering signal in both space (amplitude shown in the 2-D histograms of Figures 1c and 1d) and time (Figure 3e).

Seasonality in KE variance is similar for both WBCs (Figures 3c and 3d), with a clear summer intensification near the diurnal period, corresponding to the stronger summer land/sea breeze (Figures 3a and 3b). For periods up to ~ 10 days wind forcing may still be the primary driver of current fluctuations; the FC exhibits more variability during winter and the EAC during summer, which matches local wind variability. For periods longer than ~ 10 days, summer variance is larger than winter, in contrast to local wind. In the EAC, near-bottom ocean currents measured at mooring CH100 (Figure 1d) do not show any seasonal change in energy across the internal wave band, with the exception of diurnal and semidiurnal peaks, which are larger during winter (Figure 3f). This contrasts with both the surface currents and the summer peak in wind forcing, suggesting that surface currents exhibit seasonal wind-driven fluctuations not observed near the bottom. At periods above 10 days, surface and near-bottom currents exhibit the same summer intensification, in direct contrast to wind forcing, suggesting an internal ocean signal not driven by the local wind (Schaeffer et al., 2014).

3.3. Spatial Variability of Currents

Wavenumber spectra in geographical coordinates contain more energy than in jet coordinates at the larger scales ($> \sim 15$ km), and less at the smaller scales ($< \sim 15$ km), although the mean slopes are not substantially different between coordinate frames (Figure 4). This is because the geographical time-mean, which is used

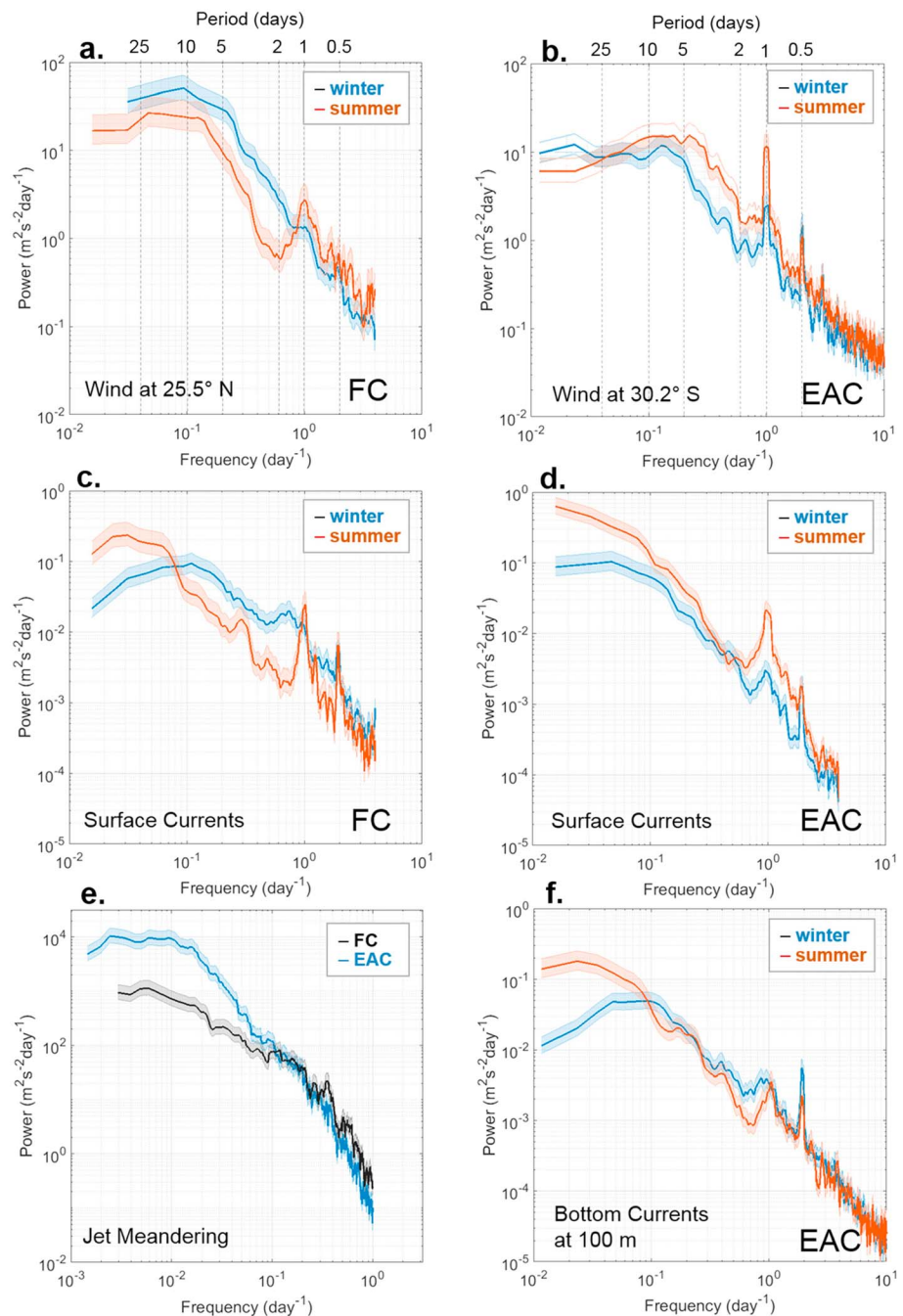


Figure 3. Kinetic energy frequency power spectra. (a) Wind at 25.5°N off Miami, FL; (b) wind at 30.2°S at Coffs Harbour; (c) FC surface currents at grid cell 25.36°N, 80.02°W; (d) EAC surface currents at grid cell 31.31°S, 153.19°E corresponding to mooring CH100; (e) FC and EAC meandering time series; (f) mooring CH100 bottom currents at 100-m isobath (measured at 89 m). The shading denotes 95% confidence intervals.

to obtain the fluctuating flow field, has spread the energy of the jet in space (Figure 2a), leading to higher variability at the larger scales, and less at small scales.

In jet coordinates, mean EKE wavenumber spectral slopes are -2.6 in the FC and -3.2 in the EAC (Figure 4). The steeper EAC slope is due to higher variability in the mesoscale range (> 15 km; Schaeffer et al., 2014). Even though we control for lateral movement of the WBCs in jet coordinates, there are still structural variations due to meandering and associated eddying that influence the spectra. Spectra of divergent motions were weak in

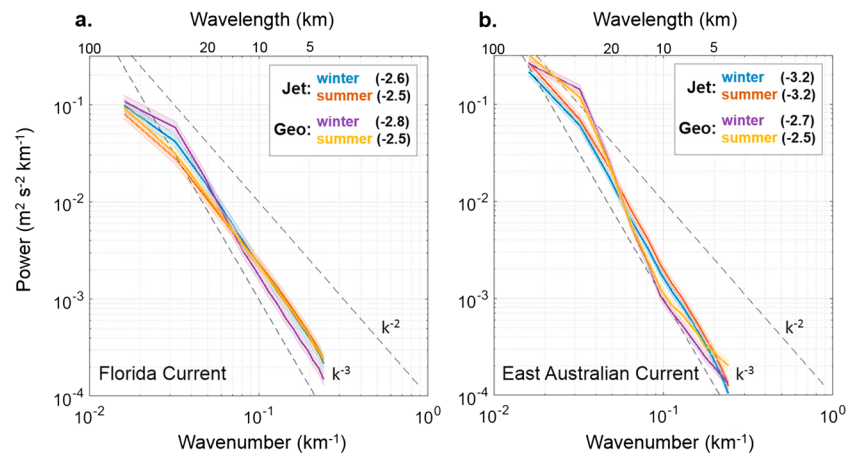


Figure 4. Eddy kinetic energy 1-D wavenumber power spectrum. Numbers in parentheses denote the mean slope of the line across all wavenumbers. The shading denotes 95% confidence intervals.

both WBC regions (not shown), where flow is dominated by the rotational component. In both WBCs, there is weak seasonality at submesoscales, and only in the FC is there a marginal winter increase in variance above ~15 km.

4. Discussion

Whereas previous studies qualitatively compared WBCs (e.g., Szabo & Weatherly, 1979) this is the first time that two WBCs have been examined using analogous data sets in an objective frame of reference that controls for the meandering signal. By converting to a jet-following coordinate frame, we find that the time-mean velocity and shear profiles of the two WBC jets are remarkably similar. Rossby and Zhang (2001) showed the Gulf Stream velocity profile near 70°W can be modeled with two back-to-back exponentials, which have scale-widths of comparable length to the Rossby radius of deformation set by the depth of the pycnocline. We fitted an exponential function to the cyclonic shear region of the velocity profiles (Figure 2c; ignoring 10 km about the rounded jet core), obtaining scale-widths of 24 and 16 km in the FC and EAC, respectively. These scale-widths match quite well existing observations of Rossby deformation radii in the cyclonic shear region of the WBCs: ~15–30 km in the Florida Straits (Shay et al., 2000) and ~15 km in the Tasman Sea (Schaeffer et al., 2014).

Nonetheless, differences still exist between the two WBCs. The EAC has a more energetic eddy field, evident in the frequency and wavenumber spectra (Figures 3 and 4). This is at least partly due to contrasting coastlines: at 25°N, the FC is constrained within a channel and unable to sustain large meanders, and mesoscale eddies that form upstream are sheared apart as they are advected through the narrowing and shoaling channel (Fratantoni et al., 1998). In contrast, the EAC is unimpeded to the east and susceptible to large-amplitude displacements offshore by the advection of mesoscale cyclonic eddies along its inshore flank (Roughan et al., 2017). Indeed, the EAC system is unique among WBCs for its large EKE-to-KE ratio (Boland & Hamon, 1970; Godfrey et al., 1980).

Both upstream WBC regions exhibit an approximate k^{-3} power law in the EKE wavenumber spectra. The observed slopes are similar to those reported by Callies and Ferrari (2013) in the Gulf Stream extension but steeper than in the Kuroshio ($k^{-2.3}$; Qiu et al., 2017) and in the subtropical North Pacific (k^{-2} ; Callies & Ferrari, 2013). From a global survey of mesoscale wavenumber spectra, Xu and Fu (2011) showed that the steepest slopes are over WBC regions. In the coastal ocean, Lekien and Coulliette (2007) found k^{-3} using HF radar in Monterey Bay, and Soh and Kim (2018) found k^{-2} to k^{-3} from HF radar offshore San Diego. Results from a global analysis of drifter pair separation by Corrado et al. (2017) also found steep slopes down into the marginal submesoscale range (5 km). Caution should be taken when attempting to reconcile wavenumber slopes to turbulence theory (Armi & Flament, 1985); however, our results are consistent with quasigeostrophy (Charney, 1971), implying that ocean dynamics and mixing in these regions are controlled by the large-scale flow (Beron-Vera & LaCasce, 2016; Beron-Vera & Olascoaga, 2009).

In both WBCs, current variability peaks during summer at periods >10 days, in contrast to local wind forcing (Figures 3a and 3b). Increased summer EKE has been observed before in WBCs (e.g., Archer, Roughan, et al., 2017; Qiu & Chen, 2004; Ridgway & Godfrey, 1997), in phase with summer intensification of WBC jet speeds (Archer, Roughan, et al., 2017). The reason for an observed global EKE summer maximum is still debated. The prevailing theory is that seasonal changes in upper ocean stratification modulate baroclinic instability (Gill et al., 1974), which is greatest in spring when the meridional thermocline tilt is maximum (Capet et al., 2016; Qiu, 1999). Subsequent summer heating and reduced wind-driven vertical mixing flattens the thermocline, releasing available potential energy in the form of EKE (Kang & Curchitser, 2015), with a phase lag controlled by the growth rate of baroclinic mesoscale eddies (Qiu, 1999). Other proposed mechanisms include seasonal changes in dissipation, rather than production, of EKE (Duhaut & Straub, 2006).

We do not observe a distinct seasonal cycle in EKE wavenumber spectra, in contrast to recent studies that show higher energy within the submesoscale range during winter (Callies et al., 2015; Qiu et al., 2017). Submesoscale motions have a variety of generation mechanisms including mixed layer instability, direct wind forcing, or Charney instability, all of which are sensitive to surface mixing and hence show a seasonal dependence (McWilliams, 2016). However, submesoscales are also generated from frontogenesis by a mesoscale straining field or interactions with topography, which do not have any seasonal dependence. The studies above focused on open ocean areas where the mean current flow is weaker and mixed layer instabilities strengthen in winter with greater mixed layer depth. Here we resolve strong upstream WBC jets against the continental slope that undergo a weaker mixed layer depth seasonal cycle (Gula et al., 2014), with submesoscale frontal instabilities that are related to topographic interaction (Gula et al., 2015) and exhibit no seasonal cycle (Lee & Mayer, 1977; Schaeffer et al., 2017). Weak submesoscale seasonality has also been documented by Yoo et al. (2018) on the east coast of South Korea, which they attribute to the formation mechanism being mesoscale frontogenesis and topographic shear.

While this study represents the first detailed investigation of kinematic similarities between two WBCs, we are unable to investigate the underlying dynamics with only surface observations. Nonetheless, these observed commonalities can inform ocean models that resolve these features. Looking forward, we need more concurrent surface and subsurface observations to measure how WBC are changing on interannual to decadal time scales.

Acknowledgments

We thank two reviewers whose comments improved the quality of the paper. U.S. HF radar data are available from the U.S. National HF Radar Network (<http://cordc.ucsd.edu/projects/mapping/maps/>) and <http://iwave.rsmas.miami.edu/wera/>) and Fowey Rocks wind data from <http://www.ndbc.noaa.gov/>. Thanks to Jorge Martinez-Pedraja, who maintains the Florida sites. Australian HF radar and mooring data sets are available through IMOS (<http://imos.aodn.org.au/imos/>) and wind data from the Bureau of Meteorology (<http://www.bom.gov.au/>). IMOS is supported by the Australian Government through the National Collaborative Research Infrastructure Strategy and the Super Science Initiative. We thank IMOS Ocean Radar Facility for HF radar maintenance and data management. S.K. was supported by UNSW Silverstar Research Grant. R.L. was funded by the Atlantic Oceanographic and Meteorological Laboratory and Ocean Observation and Monitoring division of NOAA. F.J.B.V. was supported by the Gulf of Mexico Research Initiative as part of the Consortium for Advanced Research on Transport of Hydrocarbon in the Environment. L.K.S. gratefully acknowledges support by NOAA IOOS-supported South East Coastal Ocean Observing Regional Association through grants NA11NOS0120033 and NA16NOS0120028.

References

- Archer, M. R., Roughan, M., Keating, S. R., & Schaeffer, A. (2017). On the variability of the East Australian Current: Jet structure, meandering, and influence on shelf circulation. *Journal of Geophysical Research: Oceans*, 122, 8464–8481. <https://doi.org/10.1002/2017JC013097>
- Archer, M. R., Shay, L. K., Jaimes, B., & Martinez-Pedraja, J. (2015). Observing frontal instabilities of the Florida Current using high frequency radar. In Y. Liu, H. Kerker, & R. H. Weisberg (Eds.), *Coastal ocean observing systems* (chap. 11, pp. 179–208). London: Elsevier. <https://doi.org/10.1016/B978-0-12-802022-7.00011-0>
- Archer, M. R., Shay, L. K., & Johns, W. E. (2017). The surface velocity structure of the Florida Current in a jet coordinate frame. *Journal of Geophysical Research: Oceans*, 122, 9189–9208. <https://doi.org/10.1002/2017JC013286>
- Archer, M. R., Shay, L. K., & Martinez-Pedraja, J. (2015). Evaluation of WERA HF radar observations: Currents, winds and waves. In *Current, Waves and Turbulence Measurements (CWTM), 2015 IEEE/OES 11th* (pp. 1–9). <https://doi.org/10.1109/CWTM.2015.7098148>
- Armi, L., & Flament, P. (1985). Cautionary remarks on the spectral interpretation of turbulent flows. *Journal of Geophysical Research*, 90(C6), 11,779–11,782. <https://doi.org/10.1029/JC090iC06p11779>
- Beron-Vera, F. J., & LaCasce, J. H. (2016). Statistics of simulated and observed pair separations in the Gulf of Mexico. *Journal of Physical Oceanography*, 46(7), 2183–2199. <https://doi.org/10.1175/JPO-D-15-0127.1>
- Beron-Vera, F. J., & Olascoaga, M. J. (2009). An assessment of the importance of chaotic stirring and turbulent mixing on the West Florida Shelf. *Journal of Physical Oceanography*, 39(7), 1743–1755. <https://doi.org/10.1175/2009JPO4046.1>
- Boland, F. M., & Hamon, B. V. (1970). The East Australian Current, 1965–1968. *Deep Sea Research*, 17, 777–794. [https://doi.org/10.1016/0011-7471\(70\)90041-0](https://doi.org/10.1016/0011-7471(70)90041-0)
- Bowen, M. M., Wilkin, J. L., & Emery, W. J. (2005). Variability and forcing of the East Australian Current. *Journal of Geophysical Research*, 110, C03019. <https://doi.org/10.1029/2004JC002533>
- Bull, C., Kiss, A. E., Jourdain, N. C., England, M. H., & van Sebille, E. (2017). Wind forced variability in Eddy formation, Eddy shedding, and the separation of the East Australian Current. *Journal of Geophysical Research: Oceans*, 122, 9980–9998. <https://doi.org/10.1002/2017JC013311>
- Callies, J., & Ferrari, R. (2013). Interpreting energy and tracer spectra of upper-ocean turbulence in the submesoscale range (1–200 km). *Journal of Physical Oceanography*, 43(11), 2456–2474. <https://doi.org/10.1175/JPO-D-13-063.1>
- Callies, J., Ferrari, R., Klymak, J. M., & Gula, J. (2015). Seasonality in submesoscale turbulence. *Nature Communications*, 6(1), 6862. <https://doi.org/10.1038/ncomms7862>
- Capet, X., Roulet, G., Klein, P., & Maze, G. (2016). Intensification of upper ocean submesoscale turbulence through Charney baroclinic instability. *Journal of Physical Oceanography*, 46(11), 3365–3384. <https://doi.org/10.1175/JPO-D-16-0050.1>
- Cetina-Heredia, P., Roughan, M., Van Sebille, E., & Coleman, M. A. (2014). Long-term trends in the East Australian Current separation latitude and eddy driven transport. *Journal of Geophysical Research: Oceans*, 119, 4351–4366. <https://doi.org/10.1002/2014JC010071>

- Charney, J. G. (1971). Geostrophic turbulence. *Journal of the Atmospheric Sciences*, 28(6), 1087–1095. [https://doi.org/10.1175/1520-0469\(1971\)028<1087:GT>2.0.CO;2](https://doi.org/10.1175/1520-0469(1971)028<1087:GT>2.0.CO;2)
- Corrado, R., Lacorata, G., Palatella, L., Santoleri, R., & Zambianchi, E. (2017). General characteristics of relative dispersion in the ocean. *Scientific Reports*, 7, 46291. <https://doi.org/10.1038/srep46291>
- Cronin, M. F., Bond, N., Booth, J., Ichikawa, H., Joyce, T. M., Kelly, K., et al. (2010). Monitoring ocean-atmosphere interactions in western boundary current extensions. In J. Hall, D. E. Harrison, & D. Stammer (Eds.), *Proceedings of OceanObs'09: Sustained ocean observations and information for society, Venice, Italy, September 2009, ESA Publication WPP-306* (Vol. 2, pp. 21–25). <https://doi.org/10.5270/OceanObs09.cwp.20>
- Domingues, R., Baringer, M., & Goni, G. (2016). Remote sources for year-to-year changes in the seasonality of the Florida Current transport. *Journal of Geophysical Research: Oceans*, 121, 7547–7559. <https://doi.org/10.1002/2016JC012070>
- Ducklow, H. W., Steinberg, D. K., & Buesseler, K. O. (2001). Upper ocean carbon export and the biological pump. *Oceanography-Washington DC-Oceanography Society*, 14(4), 50–58. <https://doi.org/10.5670/oceanog.2001.06>
- Duhaut, T. H., & Straub, D. N. (2006). Wind stress dependence on ocean surface velocity: Implications for mechanical energy input to ocean circulation. *Journal of Physical Oceanography*, 36(2), 202–211. <https://doi.org/10.1175/JPO2842.1>
- Emery, W. J., & Thomson, R. E. (1998). *Data analysis in physical oceanography*. Pergamon.
- Fratantoni, P. S., Lee, T. N., Podesta, G. P., & Muller-Karger, F. (1998). The influence of Loop Current perturbations on the formation and evolution of Tortugas eddies in the southern straits of Florida. *Journal of Geophysical Research*, 103(C11), 24,759–24,779. <https://doi.org/10.1029/98JC02147>
- Gill, A. E., Green, J. S. A., & Simmons, A. J. (1974). Energy partition in the large-scale ocean circulation and the production of mid-ocean eddies. In *Deep sea research and oceanographic abstracts* (Vol. 21, pp. 499–528). Great Britain: Elsevier. [https://doi.org/10.1016/0011-7471\(74\)90010-2](https://doi.org/10.1016/0011-7471(74)90010-2)
- Godfrey, J. S., Cresswell, G. R., Golding, T. J., Pearce, A. F., & Boyd, R. (1980). The separation of the East Australian Current. *Journal of Physical Oceanography*, 10(3), 430–440. [https://doi.org/10.1175/1520-0485\(1980\)010<0430:TSOTEA>2.0.CO;2](https://doi.org/10.1175/1520-0485(1980)010<0430:TSOTEA>2.0.CO;2)
- Gula, J., Molemaker, M. J., & McWilliams, J. C. (2014). Submesoscale cold filaments in the Gulf Stream. *Journal of Physical Oceanography*, 44(10), 2617–2643. <https://doi.org/10.1175/JPO-D-14-0029.1>
- Gula, J., Molemaker, M. J., & McWilliams, J. C. (2015). Topographic vorticity generation, submesoscale instability and vortex street formation in the Gulf Stream. *Geophysical Research Letters*, 42, 4054–4062. <https://doi.org/10.1002/2015GL063731>
- Gurgel, K. W. (1994). Shipborne measurement of surface current fields by HF radar. In *OCEANS'94. 'Oceans engineering for today's technology and tomorrow's preservation.'* *Proceedings* (Vol. 3, pp. III–23). Brest, France: IEEE. <https://doi.org/10.1109/OCEANS.1994.364167>
- Gurgel, K. W., Antonischki, G., Essen, H. H., & Schlick, T. (1999). Wellen radar (WERA): A new ground-wave HF radar for ocean remote sensing. *Coastal Engineering*, 37(3-4), 219–234. [https://doi.org/10.1016/S0378-3839\(99\)00027-7](https://doi.org/10.1016/S0378-3839(99)00027-7)
- Halkin, D., & Rossby, T. (1985). The structure and transport of the Gulf Stream at 73 W. *Journal of Physical Oceanography*, 15(11), 1439–1452. [https://doi.org/10.1175/1520-0485\(1985\)015<1439:TSATOT>2.0.CO;2](https://doi.org/10.1175/1520-0485(1985)015<1439:TSATOT>2.0.CO;2)
- Imawaki, S., Bower, A., Beal, L., & Qiu, B. (2013). Western boundary currents. In G. Siedler, S. M. Griffies, J. Gould, & J. A. Church (Eds.), *Ocean circulation and climate: A 21st century perspective* (2nd ed., pp. 305–338). Oxford, UK: Elsevier Academic Press. <https://doi.org/10.1016/B978-0-12-391851-2.00013-1>
- Johns, W. E., & Schott, F. (1987). Meandering and transport variations of the Florida Current. *Journal of Physical Oceanography*, 17(8), 1128–1147. [https://doi.org/10.1175/1520-0485\(1987\)017<1128:MATVOT>2.0.CO;2](https://doi.org/10.1175/1520-0485(1987)017<1128:MATVOT>2.0.CO;2)
- Kang, D., & Curchitser, E. N. (2015). Energetics of eddy-mean flow interactions in the Gulf Stream region. *Journal of Physical Oceanography*, 45(4), 1103–1120. <https://doi.org/10.1175/JPO-D-14-0200.1>
- Kim, S. Y., & Crawford, G. (2014). Resonant ocean current responses driven by coastal winds near the critical latitude. *Geophysical Research Letters*, 41, 5581–5587. <https://doi.org/10.1002/2014GL060402>
- Kunze, E., & Toole, J. M. (1997). Tidally driven vorticity, diurnal shear, and turbulence atop Fieberling seamount. *Journal of Physical Oceanography*, 28, 811–814.
- Lee, T. N., Atkinson, L. P., & Legeckis, R. (1981). Observations of a Gulf Stream frontal eddy on the Georgia continental shelf, April 1977. *Deep Sea Research Part A. Oceanographic Research Papers*, 28(4), 347–378.
- Lee, T. N., & Mayer, D. A. (1977). Low-frequency current variability and spin-off eddies on the shelf off southeast Florida. *Journal of Marine Research*, 35(1), 193–220.
- Lekien, F., & Coulliette, C. (2007). Chaotic stirring in quasi-turbulent flows. *Philosophical transactions of the Royal Society of London A: Mathematical. Physical and Engineering Sciences*, 365(1861), 3061–3084.
- Mahadevan, A. (2016). The impact of submesoscale physics on primary productivity of plankton. *Annual Review of Marine Science*, 8(1), 161–184. <https://doi.org/10.1146/annurev-marine-010814-015912>
- Mantovanelli, A., Keating, S. R., Wyatt, L. R., Roughan, M., & Schaeffer, A. (2017). Eulerian and Lagrangian characterization of two counter-rotating submesoscale eddies in a western boundary current. *Journal of Geophysical Research: Oceans*, 122, 4902–4921. <https://doi.org/10.1002/2016JC011968>
- Martinez-Pedraja, J., Shay, L. K., Haus, B. K., & Whelan, C. (2013). Interoperability of sea-sonde and Wellen radars in mapping surface currents. *Journal of Atmospheric and Oceanic Technology*, 30(11), 2662–2675. <https://doi.org/10.1175/JTECH-D-13-00022.1>
- Mata, M. M., Tomczak, M., Wijffels, S., & Church, J. A. (2000). East Australian Current volume transports at 30 S: Estimates from the World Ocean Circulation Experiment hydrographic sections PR11/P6 and the PCM3 current meter array. *Journal of Geophysical Research*, 105(C12), 28,509–28,526. <https://doi.org/10.1029/1999JC000121>
- McWilliams, J. C. (2016). Submesoscale currents in the ocean. In *Proc. R. Soc. A*, (Vol. 472, pp. 1–32). The Royal Society. <https://doi.org/10.1098/rspa.2016.0117>
- Meinen, C. S., Baringer, M. O., & Garcia, R. F. (2010). Florida Current transport variability: An analysis of annual and longer-period signals. *Deep Sea Research Part I: Oceanographic Research Papers*, 57(7), 835–846. <https://doi.org/10.1016/j.dsr.2010.04.001>
- Mihanović, H., Pattiaratchi, C., & Verspecht, F. (2016). Diurnal sea breezes force near-inertial waves along Rottneest continental shelf, south-western Australia. *Journal of Physical Oceanography*, 46(11), 3487–3508. <https://doi.org/10.1175/JPO-D-16-0022.1>
- Paduan, J. D., & Washburn, L. (2013). High-frequency radar observations of ocean surface currents. *Annual Review of Marine Science*, 5(1), 115–136. <https://doi.org/10.1146/annurev-marine-121211-172315>
- Qiu, B. (1999). Seasonal eddy field modulation of the North Pacific subtropical countercurrent: TOPEX/Poseidon observations and theory. *Journal of Physical Oceanography*, 29, 2471–2486. [https://doi.org/10.1175/1520-0485\(1999\)029<2471:SEFMOT>2.0.CO;2](https://doi.org/10.1175/1520-0485(1999)029<2471:SEFMOT>2.0.CO;2)
- Qiu, B., & Chen, S. (2004). Seasonal modulations in the eddy field of the South Pacific Ocean. *Journal of Physical Oceanography*, 34(7), 1515–1527. [https://doi.org/10.1175/1520-0485\(2004\)034<1515:SMITEF>2.0.CO;2](https://doi.org/10.1175/1520-0485(2004)034<1515:SMITEF>2.0.CO;2)

- Qiu, B., Nakano, T., Chen, S., & Klein, P. (2017). Submesoscale transition from geostrophic flows to internal waves in the northwestern Pacific upper ocean. *Nature Communications*, 8, 14055. <https://doi.org/10.1038/ncomms14055>
- Richardson, D. E., Llopiz, J. K., Leaman, K. D., Vertes, P. S., Muller-Karger, F. E., & Cowen, R. K. (2009). Sailfish (*Istiophorus platypterus*) spawning and larval environment in a Florida Current frontal eddy. *Progress in Oceanography*, 52(4), 252–264. <https://doi.org/10.1016/j.pocean.2009.07.003>
- Richardson, W. S., Schmitz, W. J. Jr., & Niiler, P. P. (1969). The velocity structure of the Florida Current from the Straits of Florida to Cape Fear. *Deep Sea Research*, 16, 225–231.
- Ridgway, K. R., & Godfrey, J. S. (1997). Seasonal cycle of the East Australian Current. *Journal of Geophysical Research*, 102(C10), 22,921–22,936. <https://doi.org/10.1029/97JC00227>
- Rossby, T., & Zhang, H. M. (2001). The near-surface velocity and potential vorticity structure of the Gulf Stream. *Journal of Marine Research*, 59(6), 949–975. <https://doi.org/10.1357/00222400160497724>
- Roughan, M., Keating, S. R., Schaeffer, A., Cetina Heredia, P., Rocha, C., Griffin, D., et al. (2017). A tale of two eddies: The biophysical characteristics of two contrasting cyclonic eddies in the East Australian Current system. *Journal of Geophysical Research: Oceans*, 122, 2494–2518. <https://doi.org/10.1002/2016JC012241>
- Roughan, M., Schaeffer, A., & Suthers, I. M. (2015). Sustained ocean observing along the Coast of southeastern Australia: NSW-IMOS 2007–2014. In Y. Liu, H. Kerkering, & R. H. Weisberg (Eds.), *Coastal ocean observing systems* (pp. 76–98). London: Elsevier. <https://doi.org/10.1016/B978-0-12-802022-7.00006-7>
- Schaeffer, A., Gramoulle, A., Roughan, M., & Mantovanelli, A. (2017). Characterizing frontal eddies along the East Australian Current from HF radar observations. *Journal of Geophysical Research: Oceans*, 122, 3964–3980. <https://doi.org/10.1002/2016JC012171>
- Schaeffer, A., Roughan, M., & Morris, B. D. (2013). Cross-shelf dynamics in a western boundary current regime: Implications for upwelling. *Journal of Physical Oceanography*, 43(5), 1042–1059. <https://doi.org/10.1175/JPO-D-12-0177.1>
- Schaeffer, A., Roughan, M., & Wood, J. E. (2014). Observed bottom boundary layer transport and uplift on the continental shelf adjacent to a western boundary current. *Journal of Geophysical Research: Oceans*, 119, 4922–4939. <https://doi.org/10.1002/2013JC009735>
- Schott, F., Lee, T. N., & Zantopp, R. (1988). Variability of structure and transport of the Florida Current in the period range of days to seasonal. *Journal of Physical Oceanography*, 18, 1209–1230. [https://doi.org/10.1175/1520-0485\(1988\)018<1209:VOSATO>2.0.CO;2](https://doi.org/10.1175/1520-0485(1988)018<1209:VOSATO>2.0.CO;2)
- Shay, L. K., Cook, T. M., Haus, B. K., Martinez, J., Peters, H., Mariano, A. J., et al. (2000). VHF radar detects oceanic submesoscale vortex along Florida coast. *Eos, Transactions American Geophysical Union*, 81(19), 209–213. <https://doi.org/10.1029/00EO00143>
- Shay, L. K., Lee, T. N., Williams, E. J., Graber, H. C., & Rooth, C. G. H. (1998). Effects of low frequency current variability on near-inertial submesoscale vortices. *Journal of Geophysical Research*, 103(C9), 18,691–18,714.
- Shay, L. K., Martinez-Pedraja, J., Cook, T. M., Haus, B. K., & Weisberg, R. H. (2007). High frequency radar surface current mapping using WERA. *Journal of Atmospheric and Oceanic Technology*, 24(3), 484–503. <https://doi.org/10.1175/JTECH1985.1>
- Shay, L. K., Seim, H., Savidge, D., Styles, R., & Weisberg, R. H. (2008). High frequency radar observing systems in SEACOOS: 2002–2007 lessons learned. *Marine Technology Society Journal*, 42(3), 55–67. <https://doi.org/10.4031/002533208786842435>
- Shulzitski, K., Sponaugle, S., Hauff, M., Walter, K., D'Alessandro, E. K., & Cowen, R. K. (2015). Close encounters with eddies: Oceanographic features increase growth of larval reef fishes during their journey to the reef. *Biology Letters*, 11(1), 20140746. <https://doi.org/10.1098/rsbl.2014.0746>
- Simpson, J. H., Hyder, P., Rippeth, T. P., & Lucas, I. M. (2002). Forced oscillations near the critical latitude for diurnal-inertial resonance. *Journal of Physical Oceanography*, 32(1), 177–187. [https://doi.org/10.1175/1520-0485\(2002\)032<0177:FONTCL>2.0.CO;2](https://doi.org/10.1175/1520-0485(2002)032<0177:FONTCL>2.0.CO;2)
- Sloyan, B. M., Ridgway, K. R., & Cowley, R. (2016). The East Australian Current and property transport at 27°S from 2012 to 2013. *Journal of Physical Oceanography*, 46(3), 993–1008. <https://doi.org/10.1175/JPO-D-15-0052.1>
- Soh, H. S., & Kim, S. Y. (2018). Diagnostic characteristics of submesoscale coastal surface currents. *Journal of Geophysical Research: Oceans*, 123, 1838–1859. <https://doi.org/10.1002/2017JC013428>
- Szabo, D., & Weatherly, G. L. (1979). Energetics of the Kuroshio south of Japan. *Journal of Marine Research*, 37, 531–556.
- Wyatt, L. R., Mantovanelli, A., Heron, M. L., Roughan, M., & Steinberg, C. R. (2017). Assessment of surface currents measured with high-frequency phased-array radars in two regions of complex circulation. *IEEE Journal of Oceanic Engineering*, 43(2), 484–505. <https://doi.org/10.1109/JOE.2017.2704165>
- Xu, Y., & Fu, L. L. (2011). Global variability of the wavenumber spectrum of oceanic mesoscale turbulence. *Journal of Physical Oceanography*, 41(4), 802–809. <https://doi.org/10.1175/2010JPO4558.1>
- Yoo, J. G., Kim, S. Y., & Kim, H. S. (2018). Spectral descriptions of submesoscale surface circulation in a coastal region. *Journal of Geophysical Research: Oceans*. <https://doi.org/10.1029/2016JC012517>
- Yu, L., & Weller, R. A. (2007). Objectively analyzed air-sea heat fluxes for the global ice-free oceans (1981–2005). *Bulletin of the American Meteorological Society*, 88(4), 527–540. <https://doi.org/10.1175/BAMS-88-4-527>